

Optimal Vibration Control of a Constrained Damping Structure Based on the BESO Method

Shenfang Li, Rongjiang Tang, Weiguang Zheng, Yong Zhang, Zhe Feng, and Yongyou Wei

Abstract—Constrained damping materials have been widely used for vibration control of thin-walled parts. However, in some projects, it is necessary to limit the weight of thin-walled parts to achieve a lightweight design. Therefore, it is necessary to obtain the best vibration suppression effect for the thin-walled parts with a given constrained damping volume. This paper proposes a method to improve the constrained damping vibration suppression effect by maximising the structural modal loss factor under a given constrained damping treatment. The virtual degree of freedom is introduced to establish a finite element model describing the dynamic performance of a constrained damping structure. With the maximum modal loss factor as the objective function, the sensitivity of the structural modal loss factor to the design variables was derived using a differential method based on the modal strain energy of the structure. Considering the volume of the material as a constraint, the optimal layout of the damping material is searched by using the BESO (bi-directional evolutionary structural optimization) method. The accuracy of the topology optimisation results is verified through experiments. The experimental results show that the optimised damping arrangement can improve the vibration suppression effect on the plate. This method can effectively reduce the volume of the restrained damping, reduce the weight of the structure, and improve the vibration suppression performance of the structure. At the same time, this method can be extended to the vibration control of thin-walled parts of cars, aircraft cabins, and submarine shells.

Index Terms—finite element, topology optimisation, viscoelastic material, BESO method

I. INTRODUCTION

Vibration can be useful in many areas, such as piano vibrations producing pleasant sounds, and loudspeaker

vibrations producing sounds. But in many other areas, vibration is not desired, producing harmful noise and damaging machines. For example, thin-walled parts of automobile bodies vibrate due to the excitation of the power system; this means that radiative noise inside the vehicle deteriorates the acoustic characteristics of the vehicle [1]-[3]. Therefore, in some engineering fields, it is necessary to reduce vibration. The deformation of the viscoelastic layer of a constrained damping material can dissipate the vibration energy of the thin plate and reduce its vibration level, giving a superior vibration suppression performance. Therefore, constrained damping materials are commonly used in lightweight designs to suppress the vibration levels of thin-walled automobile aircraft parts [4,5]. The composition and deformation of a constrained damping structure are depicted in Fig. 1.

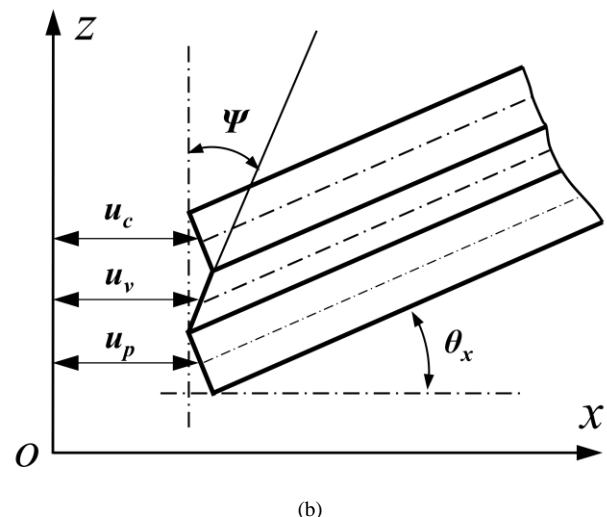
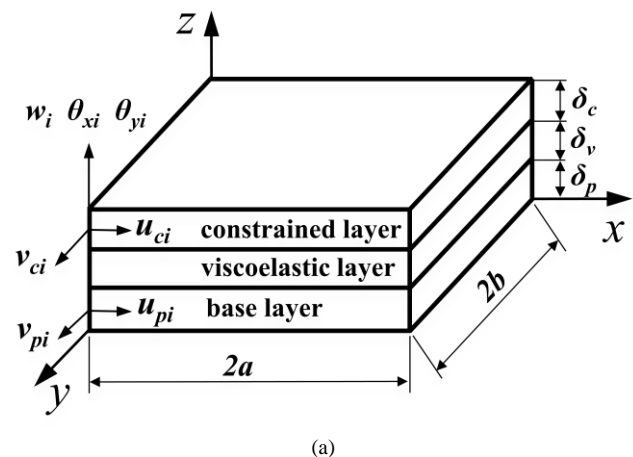


Fig. 1. The element of the constrained damping plate, (b) the deformation relationship of each constrained damping plate layer

Manuscript received August 01, 2020; revised February 07, 2021. This work was supported by the Guangxi Youth Science Fund Project (No. 2018GXNSFBA281012); the Innovation-Driven Development Special Fund Project of Guangxi (No. Guike AA19182004); the Liuzhou Scientific Research and Planning Development Project (No. 2018AA20301).

S. F. Li is a Postgraduate of the School of Mechanical and Electrical Engineering, Guilin University of Electronic Technology, Guilin 541004 China (e-mail: sanford_lee@163.com).

R. J. Tang is an Associate Professor of the School of Mechanical and Electrical Engineering, Guilin University of Electronic Technology, Guilin 541004 China (corresponding author; phone: +86 0773-3569399; e-mail: tangrongjiang@guet.edu.cn).

W. G. Zheng is an Associate Professor of the School of Mechanical and Electrical Engineering, Guilin University of Electronic Technology, Guilin 541004 China (e-mail: weiguang.zheng@foxmail.com).

Y. Zhang is an Associate Professor of the Tianjin Electronic Information College, Tianjin 300350 China (e-mail: wanghuihangyong@163.com).

Z. Feng is an Engineer of the Dong Feng Liuzhou Automobile Co., Ltd., Liuzhou 545005 China (e-mail: fengz@dfzm.com).

Y.Y. Wei is an Engineer of the Dong Feng Liuzhou Automobile Co., Ltd., Liuzhou 545005 China (e-mail: weiy@dfzm.com).

The characteristics of constrained damping structures have been researched. Huang [6] established the finite element model of the three-layer sandwich beam with a viscoelastic core. The researcher analysed the vibration and damping characteristics of the first three modes of the sandwich beam. Based on the Donnell assumptions and the linear viscoelastic theory, Zheng [7] established the dynamic equation of the multilayer passive constrained layer damping cylindrical shell. Further, the researcher analysed the dynamic characteristics of the cylindrical shell, including natural frequency, loss factor, and frequency response. Strain energy is an important indicator for evaluating the deformation of elements, and is often used to guide the reduction of structural vibration levels. Kumar [8] used the MSE (modal strain energy) method to design a layout strategy for the constrained damping patch. The coverage of the damping patch is the position where the modal strain energy is the largest in a particular mode. Lepoittevin [9] uses the modal strain energy method to estimate the damping efficiency, and propose a new method to enhance the damping performance of the segment of constrained damping material. This improves the vibration suppression effect of constrained damping in a large frequency range. Alaimo [10] provides an effective modal damping ratio calculation method based on the modal strain energy, that is, the modal damping ratio is calculated using the undamped modal result. Yuan [11] studied the vibration reduction problem of the shell through the structural modal loss factor of the multi-mode weight coefficient.

Topology optimisation methods have been widely used in structure optimisation designs. Similarly, scholars have conducted much research on the topology optimisation of constrained damping structures. By maximizing the modal loss factor as the goal, the SIMP (solid isotropic material with penalization) method and MMA (method of moving asymptotes) method are consistently used to search the optimal topology of constrained damping on the plate [12]-[14]. However, it is challenging to obtain a clear boundary configuration due to the limitations of the SIMP method. In the case of a large penalty factor, an optimal solution that is almost completely ineffective may be obtained according to a given optimisation algorithm. Ansari [15] uses the level set method to find the optimal shape and position of the constrained damping patch. The modal loss factor of the system can be maximised with the least constrained damping to achieve the best vibration suppression effect. The ESO (evolutionary structural optimisation) algorithm is simpler and easier to implement than the level set method [16,17]. This algorithm has been widely used in optimisation problems, such as stress, displacement, stiffness, and vibration frequency. Li [18] introduced the ESO method in the design of the constrained damping layout of simply supported beams. The target modal damping ratio is maximised by gradually deleting the elements with low utilisation. The BESO (bi-directional evolutionary structural optimisation) method is an improvement from the ESO method [19]. The improved method can delete and add materials, making the material layout more reasonable, and the final optimisation result more scientific. Wang [20] introduced a global stress measurement function and applied the BESO method to reduce the stress concentration effect at the corner of the L-shaped beam. Xu [21] realised the

simultaneous design of the composite macrostructure flexibility and periodic microstructure with multi-phase materials by using the BESO method. Many studies have applied the BESO method to the stiffness topology and stress topology of the structure, but less research has been undertaken in constrained damping topology. Constrained damping is widely used in vibration damping design of thin-walled structures, but it is necessary to limit the volume of constrained damping in lightweight designs. Therefore, it is necessary to study constrained damping topology based on the BESO method.

This paper studies the problem of using the BESO method to determine the optimal topology of the constrained damping layout to reduce the vibration response of the structure. Firstly, the energy method can derive the motion control equation of the constrained damping plate. Further, a mathematical model of topology optimisation of the constrained damping plate is established by combining the motion control equation with the BESO algorithm. In the mathematical model, the damping element is used as the design variable, the maximum modal loss factor of the constrained damping structure is set as the target, and the material volume is the constraint. The sensitivity of the modal loss factor to the design variables is derived from the modal strain energy of the element. The optimisation process of the BESO algorithm is developed, and the optimal distribution problem of the constrained damping material with a maximum modal loss factor is studied.

The remaining parts of this paper are organised as follows. The second section establishes the finite element model of the constrained damping plate and derives the motion control equation. The third section analyses the sensitivity of the damping elements and the optimisation criterion of the constrained damping plate based on the BESO method. In the fourth section, two numerical examples of constrained damping plates are analysed and discussed. The penultimate section provides experimental verification and the final section gives a summary of the paper.

II. CONSTRAINED DAMPING PLATE FINITE ELEMENT MODEL

A. The damping element and displacement relationship

The constrained damping element model in Fig. 1 consists of a constrained layer, a viscoelastic layer, and a base layer (in order from top to bottom). In finite element modelling, the following assumptions are made: the shear deformation of the constrained layer and the base layer is ignored; the moment of inertia is not counted; the lateral displacement and the rotation angle of any point in the same section are the same; the displacement between the layers is completely continuous, that is, there is no relative sliding between the layers; the shear modulus of the viscoelastic material is represented by a complex constant modulus $G_v^* = G_v(1 + i\eta_v)$, where G_v , η_v , and i are the real shear modulus, material loss factor of the viscoelastic material and complex unit, respectively. The plane displacements of the top and bottom tips of the viscoelastic layer in the x -direction in Fig. 1(b) are [22]:

$$\begin{cases} u_1 = u_c + \frac{\delta_c}{2} \frac{\partial \omega}{\partial x}, \\ u_2 = u_p - \frac{\delta_p}{2} \frac{\partial \omega}{\partial x}. \end{cases} \quad (1)$$

The angle of rotation of the viscoelastic layer around the y axis is:

$$\psi = \frac{u_1 - u_2}{\delta_v} \quad (2)$$

The shear strain and the x-direction plane displacement of the viscoelastic layer around the y-axis are:

$$\beta_x = \frac{u_c - u_p}{\delta_v} - \frac{d}{\delta_v} \frac{\partial \omega}{\partial x} \quad (3)$$

$$u_v = \frac{1}{2} \left[(u_c + u_p) + \left(\frac{\delta_c - \delta_p}{2} \right) \frac{\partial \omega}{\partial x} \right] \quad (4)$$

where δ_c , δ_v , and δ_p are the thicknesses of the constrained layer, the viscoelastic layer, and the base layer, respectively. u_c and u_p are the displacements of the constrained layer and the base layer in the x-direction. $d = \delta_v + \frac{\delta_c}{2} + \frac{\delta_p}{2}$, where d is the distance from the neutral surface of the base layer to the neutral surface of the constrained layer.

The shear strain and y-direction plane displacement of the viscoelastic layer around the x-axis are:

$$\beta_y = \frac{v_c - v_p}{\delta_v} - \frac{d}{\delta_v} \frac{\partial \omega}{\partial y} \quad (5)$$

$$v_v = \frac{1}{2} \left[(v_c + v_p) + \left(\frac{\delta_c - \delta_p}{2} \right) \frac{\partial \omega}{\partial y} \right] \quad (6)$$

where v_c and v_p are the displacements of the constrained layer and the base layer in the y-direction, respectively.

B. Shape functions

A rectangular element model of a damper plate containing four physical nodes is established, and each physical node contains seven degrees of freedom. The seven degrees of freedom of each node are u_c , v_c , u_p , v_p , w , θ_x , and θ_y , which represent the x- and y-direction displacements in the rectangular element of the constrained layer, the x- and y-direction displacement in the rectangular element of the base layer, the lateral displacement of the rectangular element, and the rotation angle of the neutral plane around the x- and y-axis, respectively. The interpolation functions for each degree of freedom are as follows [23]:

$$\begin{aligned} u_c &= a_1 + a_2x + a_3y + a_4xy, \\ v_c &= a_5 + a_6x + a_7y + a_8xy, \\ u_p &= a_9 + a_{10}x + a_{11}y + a_{12}xy, \\ v_p &= a_{13} + a_{14}x + a_{15}y + a_{16}xy, \\ w &= a_{17} + a_{18}x + a_{19}y + a_{20}x^2 + a_{21}xy + a_{22}y^2 \\ &\quad + a_{23}x^3 + a_{24}x^2y + a_{25}xy^2 + a_{26}y^3 \\ &\quad + a_{27}x^3y + a_{28}xy^3, \\ \theta_x &= \frac{\partial \omega}{\partial y}, \\ \theta_y &= \frac{\partial \omega}{\partial x}. \end{aligned} \quad (7)$$

The displacement vector of the rectangular element of the damping plate is

$$u = [u_1 \quad u_2 \quad u_3 \quad u_4]^T \quad (8)$$

where $u_i = [u_{ci} \quad v_{ci} \quad u_{pi} \quad v_{pi} \quad w_i \quad \theta_{xi} \quad \theta_{yi}]$, $i = 1, 2, 3, 4$.

Substituting the coordinates of the damping element nodes into (7), the following expression can be obtained:

$$\begin{aligned} u_c &= \sum_{i=1}^4 n_i u_{ci}, \quad v_c = \sum_{i=1}^4 n_i v_{ci}, \\ u_p &= \sum_{i=1}^4 n_i u_{pi}, \quad v_p = \sum_{i=1}^4 n_i v_{pi}, \\ w &= \sum_{i=1}^4 n_{\omega i} w_i, \quad \theta_x = \sum_{i=1}^4 n_{\omega i, x} \theta_{xi}, \\ \theta_y &= \sum_{i=1}^4 n_{\omega i, y} \theta_{yi}. \end{aligned} \quad (9)$$

where n_i is the plane displacement shape function of the nodes (x_i, y_i) , $n_{\omega i}$ is the lateral displacement w at the node (x_i, y_i) , and $n_{\omega i, x}$ and $n_{\omega i, y}$ are the rotation angle function around the x- and y-axis, respectively. This is expressed as:

$$\begin{aligned} n_i &= \frac{1}{4} \left(1 + \frac{x}{x_i} \right) \left(1 + \frac{y}{y_i} \right), \\ n_{\omega i} &= \frac{1}{8} \left(1 + \frac{x}{x_i} \right) \left(1 + \frac{y}{y_i} \right) \left(2 + \frac{x}{x_i} + \frac{y}{y_i} - x^2 - y^2 \right), \\ n_{\omega i, x} &= \frac{1}{8} x_i \left(1 + \frac{x}{x_i} \right)^2 \left(\frac{x}{x_i} - 1 \right) \left(\frac{y}{y_i} + 1 \right) a, \\ n_{\omega i, y} &= \frac{1}{8} y_i \left(1 + \frac{y}{y_i} \right)^2 \left(\frac{y}{y_i} - 1 \right) \left(\frac{x}{x_i} + 1 \right) b. \end{aligned} \quad (10)$$

where x_i and y_i are the coordinates of node i , respectively. a and b are half of the length of each of the elements, respectively.

The displacement of any point in an element can be obtained by interpolation of the element node displacement vector,

$$[u_c \quad v_c \quad u_p \quad v_p \quad w \quad \theta_x \quad \theta_y] = Nu \quad (11)$$

where $N = [N_1 \quad N_2 \quad N_3 \quad N_4 \quad N_5 \quad N_6 \quad N_7]^T$ are the shape functions of u_c , v_c , u_p , v_p , w , θ_x , θ_y , respectively.

From the shape function N and (4) and (6), the displacement shape functions u_v , v_v of the viscoelastic layer can be obtained

$$N_8 = \frac{1}{2} \left[(N_1 + N_3) + \left(\frac{\delta_c - \delta_p}{2} \right) (-N_7) \right] \quad (12)$$

$$N_9 = \frac{1}{2} \left[(N_2 + N_4) + \left(\frac{\delta_c - \delta_p}{2} \right) (-N_6) \right] \quad (13)$$

From the shape function N , and (3) and (5), the shear deformation shape functions β_x , and β_y of the viscoelastic layer can be obtained

$$N_{10} = \frac{1}{\delta_v} \left[(N_1 - N_3) + \left(\frac{\delta_c - \delta_p}{2} \right) (-N_7) \right] \quad (14)$$

$$N_{11} = \frac{1}{2} \left[(N_2 - N_4) + \left(\frac{\delta_c - \delta_p}{2} \right) (-N_6) \right] \quad (15)$$

C. Element motion equations

According to the plates and shells theory of elasticity, the kinetic energy and strain potential energy of each layer of the damper plate elements are derived from the energy method. The element kinetic energy of each layer is calculated using the element function as follows:

Base layer

$$\begin{aligned} E_{k,p} &= \frac{1}{2} \dot{u}^T [\rho_p \int_0^a \int_0^b \int_{-\frac{\delta_p}{2}}^{\frac{\delta_p}{2}} (N_3^T N_3 + N_4^T N_4 \\ &\quad + N_5^T N_5) dx dy dz] \dot{u} = \frac{1}{2} \dot{u}^T m_p \dot{u}. \end{aligned} \quad (16)$$

Constrained layer

$$E_{k,c} = \frac{1}{2} \dot{u}^T [\rho_c \int_0^a \int_0^b \int_{-\frac{\delta_c}{2}}^{\frac{\delta_c}{2}} (N_1^T N_1 + N_2^T N_2 + N_5^T N_5) dx dy dz] \dot{u} = \frac{1}{2} \dot{u}^T m_c \dot{u} . \quad (17)$$

Viscoelastic layer

$$E_{k,c} = \frac{1}{2} \dot{u}^T [\rho_v \int_0^a \int_0^b \int_{-\frac{\delta_v}{2}}^{\frac{\delta_v}{2}} (N_8^T N_8 + N_9^T N_9 + N_5^T N_5) dx dy dz] \dot{u} = \frac{1}{2} \dot{u}^T m_v \dot{u} . \quad (18)$$

In the above formula, \dot{u} is the first derivative of the element displacement vectors. ρ_p , ρ_v , and ρ_c are the material densities of the base layer, the viscoelastic layer, and the constrained layer, respectively. The elastic potential energy of the viscoelastic layer is divided into two parts, the in-plane potential energy and the out-of-plane potential energy. The elastic potential energy of each layer is calculated as follows:

Base layer

$$E_{p,p} = \frac{1}{2} u^T (\delta_p \int_0^a \int_0^b B_p^T D_p B_p dx dy dz + \frac{\delta_p^3}{12} \int_0^a \int_0^b B^T D_p B dx dy dz) u = \frac{1}{2} u^T k_p u . \quad (19)$$

Constrained layer

$$E_{p,c} = \frac{1}{2} u^T (\delta_c \int_0^a \int_0^b B_c^T D_c B_c dx dy dz + \frac{\delta_c^3}{12} \int_0^a \int_0^b B^T D_c B dx dy dz) u = \frac{1}{2} u^T k_c u . \quad (20)$$

The in-plane potential energy of the viscoelastic layer

$$E_{p,v} = \frac{1}{2} u^T (\delta_v \int_0^a \int_0^b B_v^T D_v B_v dx dy dz + \frac{\delta_v^3}{12} \int_0^a \int_0^b B^T D_v B dx dy dz) u = \frac{1}{2} u^T k_v u . \quad (21)$$

The out-of-plane potential energy of the viscoelastic layer

$$E_{p,v\beta} = \frac{1}{2} u^T \left[\frac{G}{\delta_v} \int_0^a \int_0^b (N_{10}^T N_{10} + N_{11}^T N_{11}) dx dy \right] u = \frac{1}{2} u^T k_{v\beta} u . \quad (22)$$

In the above formula, B is the geometric matrix of the damping elements, and D_p , D_c , and D_v are the elastic coefficient matrix of the base layer, the constrained layer, and the viscoelastic layer, respectively.

Lagrange's equation [24] is used to derive the element motion control equation of the damper plate, which is expressed as follows:

$$m_i \ddot{u} + k_i u = f_i . \quad (23)$$

where f_i is a unit excitation force. m_i , and k_i are the mass matrix and stiffness matrix of the element, respectively, where $m_i = m_p + m_c + m_v$, and $k_i = k_p + k_c + k_v + k_{v\beta}$.

The element stiffness matrix and the mass matrix are assembled into a total stiffness matrix and a total mass matrix. According to finite element theory, the total stiffness matrix and the total mass matrix are given as

$$M = \sum_{i=1}^m (m_p^i + m_c^i + m_v^i) . \quad (24)$$

$$K = \sum_{i=1}^m (k_p^i + k_c^i + k_v^i + k_{v\beta}^i) . \quad (25)$$

III. TOPOLOGY OPTIMISATION OF THE BESO METHOD

A. Mathematical models

Under the limited amount of constrained damping material, maximising the modal loss factor of the damping structure can cause the constrained damping to exhibit a better vibration suppression effect. The BESO method is based on the existence state of the elements, and continuously deletes the inefficient elements to maximise the objective function. The mathematical model of the constrained damping topology optimisation based on the BESO method is expressed as follows [25]:

$$\begin{cases} \text{find: } x = \{x_1, x_2, x_3, \dots, x_n\}^T, \\ \text{max: } \eta_r, \\ \text{subject to: } V^* - \sum_{i=0}^n V_i x_i = 0, \\ (K_r - \lambda_r M_r) \phi_r = 0, \\ x_i = \{x_{min}, 1\}. \end{cases} \quad (26)$$

where x_i is the i -th element existence state, x_{min} indicates that the element has been deleted, and 1 indicates the element exists. n is the number of damping elements, η_r is the modal loss factor of the damping structure, V^* indicates the material usage constraint, and V_i indicates the volume of the i -th element. K_r , and M_r represent the r -th order stiffness matrix and the mass matrix, respectively. λ_r , and ϕ_r are the r -th eigenvalues and eigenvectors of the structure, respectively.

B. Sensitivity analysis

According to the modal strain energy method, the r -th modal loss factor of the constrained damping structure is [26]

$$\eta_r = \eta_v \frac{U_{vr}}{U_{ar}} . \quad (27)$$

where η_v , U_{vr} , and U_{ar} are the material loss factor, the r -th order modal strain energy of the viscoelastic layer, and the r -th order total modal strain energy of the structure, respectively.

Solving the partial derivative of η_r with respect to the design variable x_i , we have

$$\frac{\partial \eta_r}{\partial x_i} = \eta_v \frac{\frac{\partial U_{vr}}{\partial x_i} U_a - U_{vr} \frac{\partial U_{ar}}{\partial x_i}}{U_{ar}^2} . \quad (28)$$

During the optimisation process, the base layer remains intact, and the viscoelastic layer and the constrained layer are synchronously reduced. Considering that the constrained damping element is the design variable x_i and introducing the penalty factor p , the element modal strain energy and the global modal strain energy of the structure are calculated as follows:

$$U_{vr,i} = \frac{1}{2} \phi_{r,i}^T K_i^e \phi_{r,i} = x_i^p U_{vr,i}^e . \quad (29)$$

$$U_{ar} = \frac{1}{2} \phi_{a,r}^T K \phi_{a,r} = \sum_{i=1}^n x_i^p U_{cvr,i}^e + U_p \quad (30)$$

where K_i^e is the stiffness matrix of the i -th element. U_p and p are the global modal strain energy of the base layer, and the penalty factor, respectively. $\phi_{r,i}$, $U_{vr,i}^e$, and $U_{cvr,i}^e$, where $U_{cvr,i}^e = U_{vr,i}^e + U_{cr,i}^e$, are the eigenvector, the element modal strain energy of the viscoelastic layer, and the superposition of the element modal strain energy of the viscoelastic layer and the corresponding constrained layer of the i -th element of the r -th order, respectively.

Solving the partial derivative of the two sides of (29) and (30) with respect to the design variable x_i , we have

$$\frac{\partial U_{vr,i}}{\partial x_i} = p x_i^{p-1} U_{vr,i}^e \quad (31)$$

$$\frac{\partial U_{ar}}{\partial x_i} = p x_i^{p-1} U_{cvr,i}^e \quad (32)$$

Substituting (31) and (32) into (28), we have

$$\frac{\partial \eta_r}{\partial x_i} = p x_i^{p-1} \frac{\eta_v}{U_a^2} [(U_{ar} - U_{vr}) U_{vr,i}^e - U_v U_{cr,i}^e] \quad (33)$$

The element sensitivity of the BESO method can be expressed as:

$$\alpha_{r,i} = p x_i^{p-1} \frac{\eta_v}{U_a^2} [(U_{ar} - U_{vr}) U_{vr,i}^e - U_v U_{cr,i}^e] \quad (34)$$

When optimising the multi-order modal loss factor at the same time, the comprehensive element sensitivity is calculated as follows:

$$\alpha_i = \sum_{i=1}^m \omega_i \alpha_{r,i} \quad (35)$$

where ω_i , where $\sum_{i=1}^m \omega_i = 1$, is the weighting factor of each mode.

In order to avoid mesh dependence and checkerboard patterns in the topology optimisation process, the element sensitivity needs to be filtered and smoothed.

$$\bar{\alpha}_i = \frac{\sum_{j=1}^n d_{ij} \alpha_j}{\sum_{j=1}^n d_{ij}} \quad (36)$$

where $\bar{\alpha}_i$, α_j , r , and $r(i,j)$ are the sensitivity of the filtered element i , the sensitivity of the unfiltered element j , the filter radius, and the distance between the elements i and j , respectively. In addition, d_{ij} where $d_{ij} = \max\{0, r - r(i,j)\}$ is the weighting factor of the element j in the filtering radius.

In addition, in order to improve the convergence of the optimisation process, we propose using an average sensitivity such that the current k -th iteration and the sensitivity of the previous two iterations as the current sensitivity value.

$$\bar{\alpha}_i = \frac{\bar{\alpha}_i^{k-2} + \bar{\alpha}_i^{k-1} + \bar{\alpha}_i^k}{3}, k > 2 \quad (37)$$

C. Optimisation criteria of the BESO method

When topology optimisation is performed by the BESO algorithm, the design variable determined as the inefficient

element is set to a minimum value, and this element can still participate in the subsequent sensitivity filtering calculation. When a deleted element is determined to be a high-efficiency element, it needs to be restored to a physical element. The single-step target volume of the next iteration should be calculated before a new iteration. Since the target volume (V^*) can be larger or smaller than the initial estimated volume, the target volume in each iteration may gradually decrease or increase the element the target volume has reached. The single-step target volume is calculated as follows

$$V_{k+1} = V_k(1 \pm EVR), (K = 1,2,3, \dots) \quad (38)$$

where EVR is the volume evolution rate. When single-step target volume satisfies the overall volume constraint, the volume of subsequent iterations will remain invariant. That is

$$V_{k+1} = V^* \quad (39)$$

When updating element design variables, all elements are arranged into a sequence, based on the sensitivity values of the individual elements. We use two threshold parameters α_{del}^{th} and α_{add}^{th} to increase and delete elements [27].

$$x_i^{k+1} = \begin{cases} 0 & \text{if } \alpha_i \leq \alpha_{del}^{th} \text{ and } x_i^k = 1, \\ 1 & \text{if } \alpha_i > \alpha_{add}^{th} \text{ and } x_i^k = 0, \\ x_i^k & \text{otherwise.} \end{cases} \quad (40)$$

The constrained damping topology optimisation process based on the BESO method is shown in Fig. 2.

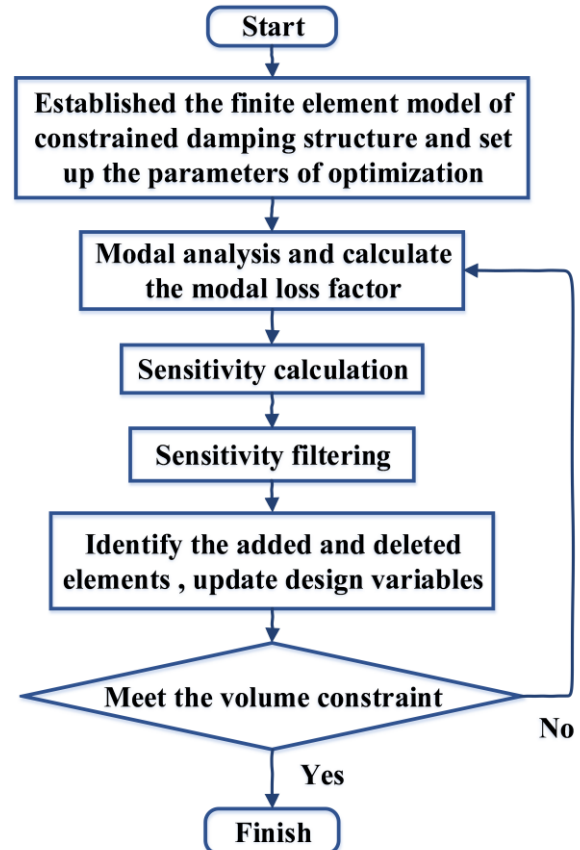


Fig. 2. The BESO method optimization process

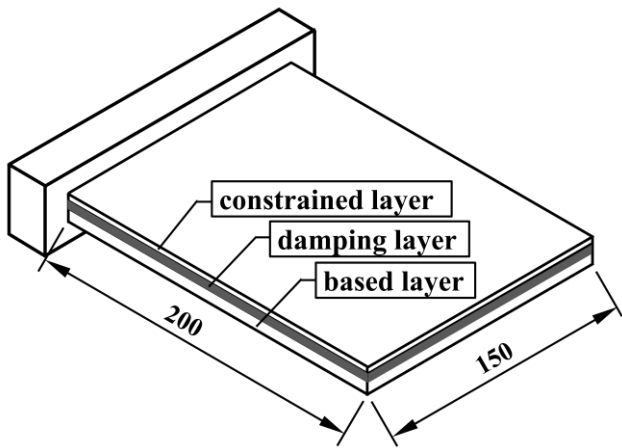


Fig. 3. A cantilever beam geometric model with full coverage constrained damping

TABLE I
MATERIAL PARAMETERS OF CONSTRAINED DAMPING OF THE
CANTILEVER BEAM

	Modulus (MPa)	Poisson ratio	Density ($\text{kg} \cdot \text{m}^{-3}$)	Material loss factor
The base layer	68900	0.3	2800	-
The viscoelastic layer	12	0.495	1300	0.5
The constrained layer	68900	0.3	2800	-

IV. NUMERICAL EXAMPLES AND DISCUSSION

In this section, we will illustrate the effectiveness of the proposed method in two cases. One is a 2D cantilever beam and the other is a rectangular plate fixed on four sides. The constrained damping is fully covered on the base plate in the initial optimisation design. In both examples, the constraint topology optimisation program based on the BESO method was developed and executed in MATLAB. The volume evolution rate EVR of the material to be removed in the iteration is set to $EVR = 1\%$. The element additions and deletions share the same set of thresholds; see the literature for further information [28].

A. Cantilever beams

A cantilever beam is a basic component in aerospace, machinery, and other areas. In these areas, there are certain requirements for the vibration response of cantilever beams. This numerical example analyses the vibration response of a cantilever beam covered with constrained damping. Fig. 3 is a schematic diagram of a full-coverage constrained-damped cantilever beam. The size of the cantilever beam is 200 mm \times 150 mm. Further, the thicknesses of the base layer, viscoelastic layer, and constrained layer are 1.5 mm, 0.5 mm, and 1 mm, respectively. The material of the viscoelastic layer is butyl damping rubber, and the constrained layer and the base layer is aluminium (the material parameters of each layer are shown in Table I). The constrained damping topology optimisation model of the cantilever beam is established by using the modelling methods shown in Sections II and III of this paper. The cantilever beam is discretised by a quadrilateral element with length $h_e = 10$ mm, and the finite element model contains 300 elements. In the finite element model, only one short side of the cantilever beam base layer

is a fixed constraint, while the viscoelastic layer and the constrained layer are free. The target volume of the constrained damping material is set to 50% of the full coverage. The constrained damping layout is optimised by maximising the modal loss factors of the first and second modes.

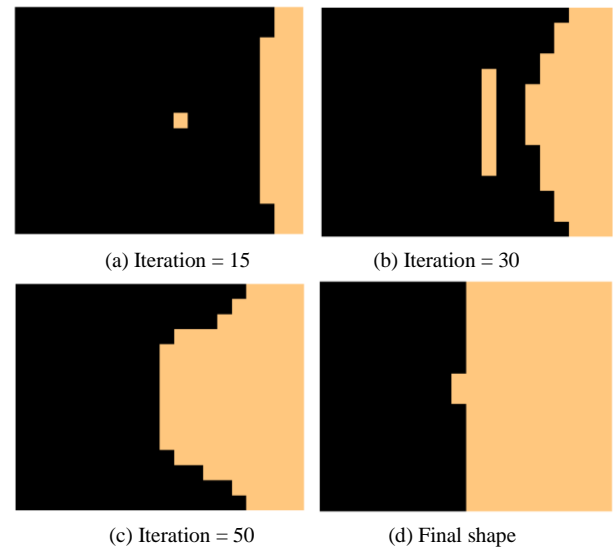


Fig. 4. The partially constrained damping layout iterative change maps of the cantilever beam at the first-order mode

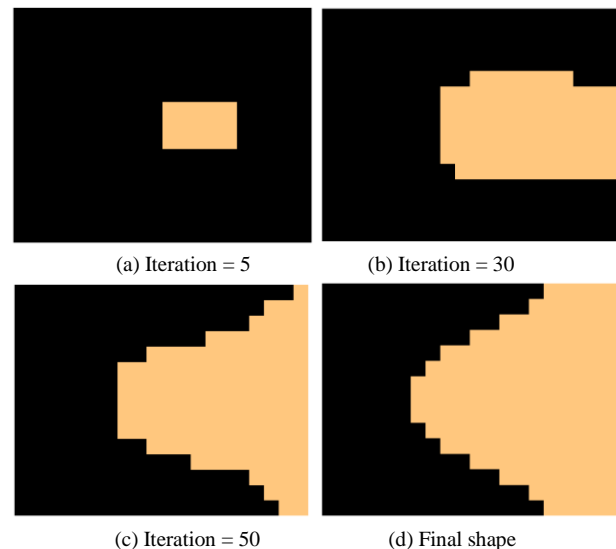


Fig. 5. The partially constrained damping layout iterative change maps of the cantilever beam at the second-order mode

Fig. 4 and 5 are the partial constrained damping layout iterative change maps aimed at maximising the modal loss factors of first- and second-order, respectively. The optimisation result is drawn by MATLAB software according to the topology optimisation program. It can be seen from Fig. 4 that the optimal distribution of constrained damping for the first-order modal loss factor is mainly distributed at one side of the constraint. The optimisation initially removes the damping material from the free short-side of the cantilever beam until the material volume constraint is met. As seen in Fig. 5, the second-order modal loss factor is optimized. Initially, the material is removed from the cantilever beam's middle part. During the optimization process, some of the deleted elements are converted into solid elements due to the recovery characteristics of the BESO method. Finally, the

remaining material is distributed on the constrained end and the edge of the cantilever beam's long side.

Fig. 6. shows the change graph for the modal loss factor. When the optimization goal is to maximize the first-order modal loss factor, the structure's modal loss factor increases first before decreasing. According to the layout change diagram in Figure 4, the elements at the cantilever beam's free end are less sensitive to the modal loss factor. They are deleted first during optimization. The elements in the middle of the cantilever beam are more sensitive to the modal loss factor. After this part of the element is deleted, the modal loss factor of the structure is reduced. Finally, the first-order modal loss factor of the cantilever beam is similar before and after optimization. When the optimization goal is to maximize the second-order modal loss factor, the structure's modal loss factor decreases slowly as the elements are deleted. After 70 iterations, some low-efficiency elements were transformed into high-efficiency elements. Further, the modal loss factor of the final structure was increased. The optimization results show that the constrained damping topology optimization technology using the BESO method can fully optimize the constrained damping's topology layout. Then, the structure maintains high vibration energy dissipation characteristics.

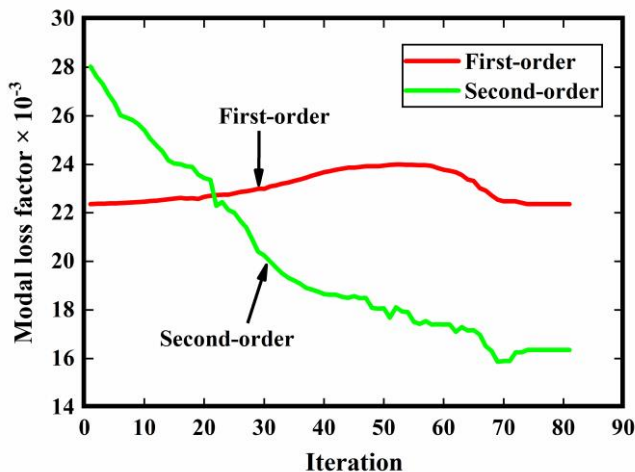


Fig. 6. The change of modal loss factor of the cantilever beam

TABLE II
THE COMPARISON CHART OF MODAL LOSS FACTOR OF THE CANTILEVER BEAM

	First-order	Second-order
Before optimisation	0.02237	0.02803
After optimisation	0.02236	0.01636
Variance ratio	-0.03%	-41.65%

Table II shows a comparison of the first- and second-order modal loss factors before and after optimisation. It can be seen from Table II that when the material usage is constrained to 50% of the full coverage, the first-order modal loss factor is slightly reduced by 0.03% after optimisation, and the second-order modal loss factor is reduced by 41.65%. By optimising the constrained damping layout, the utilisation efficiency of constrained damping is greatly improved.

B. Four-edge fixed plate

Some components in the areas of machinery and automobiles will be simplified to the model of a four-sided

fixed rectangular plate when analysing the vibration response. This numerical example analyses the vibration response of a four-sided clamped plate covered with constrained damping. Fig. 7 is the schematic diagram of a four-sided fixed rectangular plate with full coverage constrained damping. The size of the rectangular plate is 400 mm × 300 mm. The thicknesses of the base layer, the viscoelastic layer, and the constrained layer are 2 mm, 0.5 mm, and 1 mm, respectively. The material of the viscoelastic layer is a pitch-based damping material, and the material of the restraint layer and the base layer is aluminium; the material parameters of each layer are shown in Table III. The constrained damping topology optimisation model of the rectangular plate is established by using the modelling methods given in Sections II and III of this paper. The rectangular plate geometry model is discretised by a quadrilateral element with length $h_e = 10$ mm, and the finite element model contains 1200 elements. In the finite element model, the four sides of the rectangular plate base layer are a fixed constraint, and the viscoelastic layer and the constrained layer are free. The target volume of the constrained damping material is set to 50% of the full coverage. The optimisation of the constrained damping layout is optimised by maximising the modal loss factors of the first and second modes.

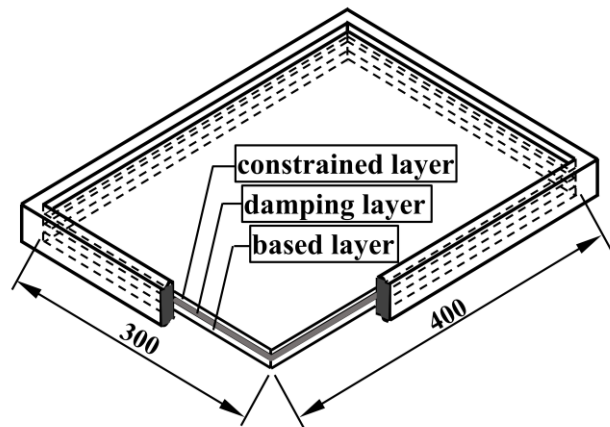


Fig. 7. A four-sided fixed rectangular plate with full coverage constrained damping

TABLE III
MATERIAL PARAMETERS OF THE CONSTRAINED DAMPING RECTANGULAR PLATE

	Modulus (MPa)	Poisson ratio	Density (kg · m ⁻³)	Material loss factor
The base layer	68900	0.3	2800	-
The viscoelastic layer	3	0.49	1000	0.5
The constrained layer	68900	0.3	2800	-

Fig. 8 and 9 are partial iterative variation diagrams of the constrained damping layout optimisation of the rectangular plate, aimed at maximising the first- and second-order modal loss factors, respectively. The optimisation result is drawn by MATLAB software according to the topology optimisation program. It can be seen from Fig. 8 that the constrained damping treatment optimised for the first-order modal loss factor of the rectangular plate is mainly distributed in the

middle of the rectangular plate. At the beginning of the optimisation, the damping material is removed from the middle and the periphery of the damping structure until the material volume constraint is satisfied. Finally, the damping material is annularly distributed in the middle of the rectangular plate. It can be seen from Fig. 9 that the optimisation is initially to remove the material from the middle and the periphery of the rectangular plate and finally, the constrained damping treatment is distributed in a double ring shape in the middle of the rectangular plate.

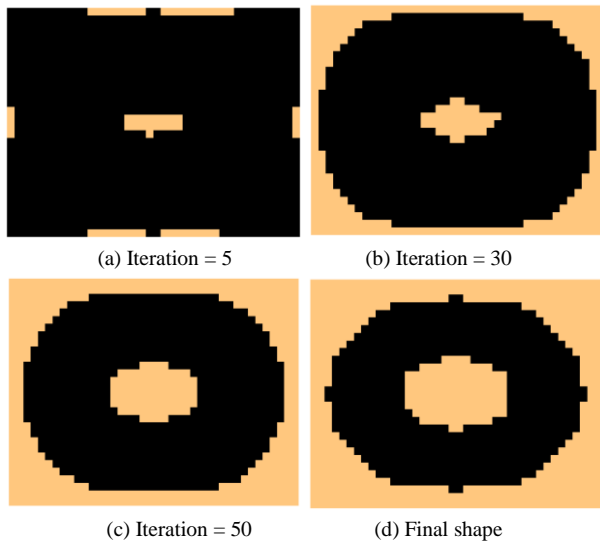


Fig. 8. The partially constrained damping layout iterative change maps of the cantilever beam at first-order mode

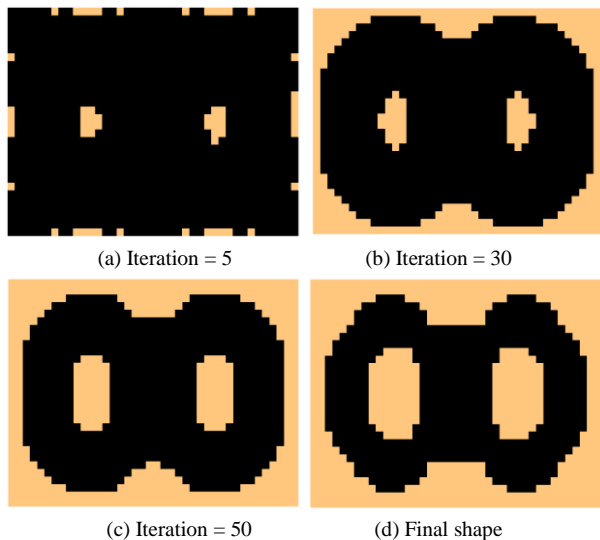


Fig. 9. The partially constrained damping layout iterative change maps of the cantilever beam at second-order mode

Fig. 10 shows a graph of the variation of modal loss factor of the rectangular plate structure. Both the first- and second-order modal loss factors decrease slowly with each iteration. According to the results of the constrained damping layout in Fig. 8, the sensitivity of the modal loss factors of the constrained damping elements around and in the middle of the rectangular plate is small when optimizing the first-order modal loss factor. Those elements are deleted in the optimization. The sensitivity of the element in the iterative calculation is changing. Some elements that have been deleted were re-converted into high-efficiency elements

during the optimization process and re-converted to solid elements, which caused the modal loss factor curve to increase during the optimization process suddenly. When optimizing the second-order modal loss factor, the structure's modal loss factor slowly decreases with the deletion of the materials, and the final modal loss factor of the structure tends to be stable.

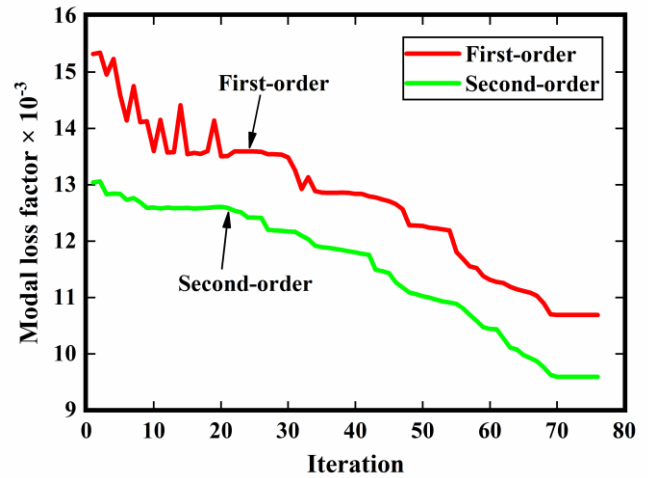


Fig. 10. The change of modal loss factor of the rectangular plate

TABLE IV
THE COMPARISON CHART OF MODAL LOSS FACTOR OF THE RECTANGULAR PLATE

	First-order	Second-order
Before optimisation	0.0153	0.0130
After optimisation	0.0107	0.0096
Variance ratio	-30.07%	-26.15%

Table IV is a comparison of the first- and second-order modal loss factors of the rectangular plate before and after optimisation. It can be seen from Table IV, that when the material usage is constrained to 50% of the full coverage, the first-order modal loss factor is reduced by 30.07% after optimisation, and the second-order modal loss factor is reduced by 26.15%. The results show that the constrained damping layout's topology optimization using the BESO method can keep the damping material with high energy dissipation characteristics under the limited amount of damping material.

V. EXPERIMENTAL VERIFICATION

In this section, the modal experimental will be performed on the results of the two numerical examples in Section IV. The equipment used includes an 8-channel LMS Teat.lab test system, a computer, an acceleration sensor, and a force hammer. The specific test plan is as follows. (1) The measurement points are arranged on the constrained damping plate. The measurement point position is the striking position of the force hammer in the experiment. (2) The computer is connected to the LMS Teat.lab test system and we ensure that both can communicate normally. The force hammer and acceleration sensor are connected to the LMS Teat.lab test system in sequence. (3) The acceleration sensor is fixed on the back of the constrained damping, and we set the relevant modal experimental parameters, such as trigger level, bandwidth, windowing, and driving points in the user interface of the LMS Test.lab test system. (4) We perform a

modal test; move the force hammer to traverse all the measurement points until the modal experimental is completed.

Fig.s 11(a)-(d) show the modal test system of the cantilever beam, the full coverage of the constrained damping, the first-order modal optimisation results, and the second-order modal optimisation results of the cantilever beam, respectively. Fig.s 12(a)-(d) show the modal test systems of the four-edge fixed plate, the full coverage of the constrained damping, the first-order modal optimisation results, and the second-order modal optimisation results of the four-edge fixed plate, respectively. This paper assumes that the loss factor and the elastic modulus of the damping material are constant. The material parameters of the cantilever beam and the four-edge fixed plate are the same as those in Tables II and III, respectively.

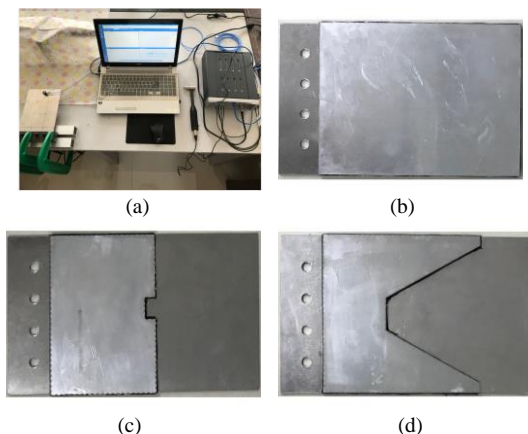


Fig. 11. (a) the modal test system of the cantilever beam, (b) the cantilever beam with full coverage constrained damping, (c) the first-order modal optimisation results of the cantilever beam, and (d) the second-order modal optimisation results of the cantilever beam

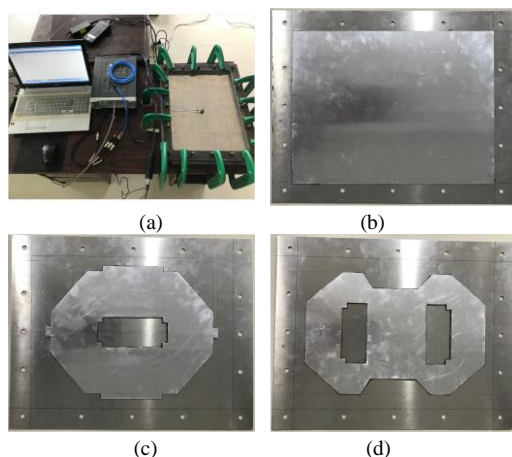


Fig. 12. (a) the modal test system of the four-edge fixed plate, (b) the four-edge fixed plate with full coverage constrained damping, (c) the first-order modal optimisation results of the four-edge fixed plate, and (d) the second-order modal optimisation results of the four-edge fixed plate

The experimental results of modal frequency and modal damping of the cantilever beam are shown in Table v. The FRF (frequency response function) of the cantilever beam between the excitation point (0 mm, 140 mm) and the response point (100 mm, 200 mm) is shown in Fig. 13. Taking the first- and second-order modal loss factors of the cantilever beam as the optimisation targets, the natural frequency of the optimised cantilever beam is larger than that of the undamped treatment. From the results of Table V and

Fig. 13, it can be seen that at the first-order modal frequency, the minimum frequency response function is at the response point of Fig. 11(b), followed by the response point of Fig. 11 (c), and finally the response point of Fig. 11(d), which shows that the first-order modal damping of the optimisation result in Fig. 11(c) has reached a maximum, and the vibration suppression at this response point is the best. Also, at the second-order modal frequency, comparing the FRF of the response points of the cantilever beams in Fig. 11(b), (c), and (d), respectively, the second-order modal damping of the optimisation result in Fig. 11(d) reaches the maximum.

The modal frequency and modal damping experimental results of the four-edge fixed plate are shown in Table VI. The FRF of the four-edge fixed plate between the excitation point (60 mm, 240 mm) and the response point (120 mm, 160 mm) is shown in Fig. 14. Taking the first-order modal loss factor of the four-edge fixed plate as the optimisation goal, the first-order natural frequency change is small. The second-order modal loss factor of the four-edge fixed plate is optimised, and the optimised second-order natural frequency is shifted to a higher frequency. From the results in Table VI and Fig. 14, comparing the FRF of the response point in Fig. 12(b), (c), and (d) at the first-order modal frequency, we can conclude that the first-order modal damping in Fig. 12(c) reaches a maximum, and the vibration suppression at this response point is best. At the second-order modal frequency, we also deduce that the second-order modal damping of Fig. 12(d) reaches a maximum.

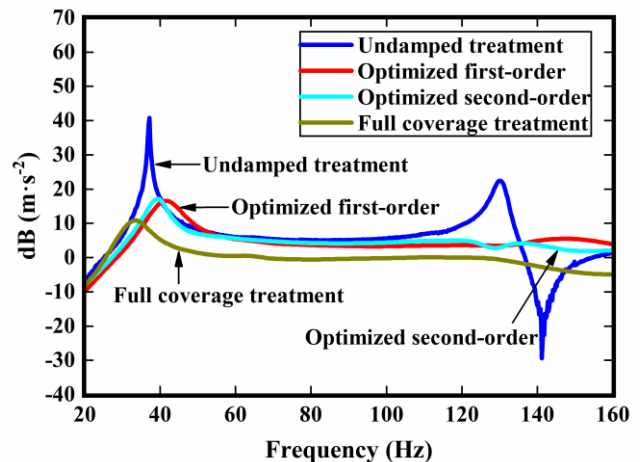


Fig. 13. The FRF of the cantilever beam

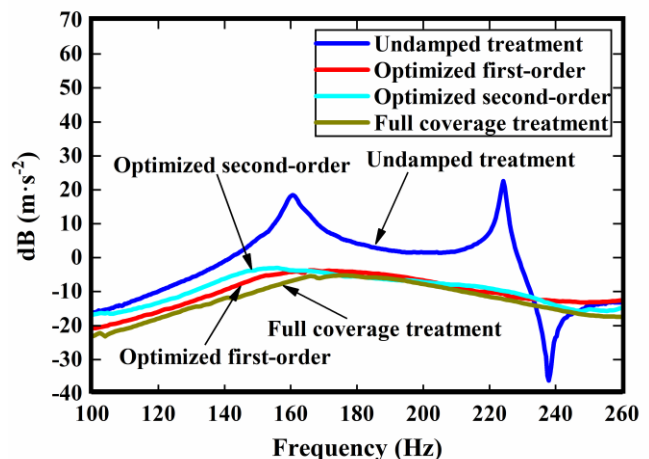


Fig. 14. The FRF of the four-edge fixed plate

TABLE V
THE MODAL FREQUENCY AND MODAL DAMPING RESULTS OF THE CANTILEVER BEAM

	The first-order		The second-order	
	modal frequency (Hz)	modal damping (%)	modal frequency (Hz)	modal damping (%)
Undamped treatment	37.003	0.45	130.267	0.95
Full coverage treatment	33.924	6.04	116.873	4.25
Optimized first-order	41.321	5.75	136.368	3.46
Optimized second-order	39.170	5.68	130.038	3.58

TABLE VI
THE MODAL FREQUENCY AND MODAL DAMPING RESULTS OF THE FOUR-EDGE FIXED PLATE

	The first-order		The second-order	
	modal frequency (Hz)	modal damping (%)	modal frequency (Hz)	modal damping (%)
Undamped treatment	160.321	0.16	224.250	0.22
Full coverage treatment	156.574	1.66	255.566	2.56
Optimized first-order	160.401	1.48	252.235	2.12
Optimized second-order	158.420	1.39	251.029	2.41

From the two experiments, we can conclude that under the constraint of 50% material consumption, the modal damping of the cantilever beam and the four-edge fixed plate reaches a maximum after the optimisation treatment. The experimental results verify the accuracy of the calculation results of the constrained damping layout optimisation with the modal loss factor as the target in the two numerical examples.

VI. CONCLUSIONS

In this paper, the thin plate with constrained damping is analysed as the research object. Meanwhile, the BESO method is used to study the topology optimisation problem of the constrained damping layout. The main content is summarised as follows:

(1) The deformation and displacement of each layer of the constrained damping element are analysed. The virtual degrees of freedom are introduced to establish the dynamic finite element equation of the damping element through the energy method. We have taken the maximisation of structural modal loss factor as the optimisation target. From this, the sensitivity of the objective function to the design variables of the damping element is deduced by the differential method. Taking the amount of damping material as the constraint condition combined with the finite element dynamics model and the BESO method, the mathematical model of topology optimisation is established.

(2) The layout of damping material is optimised for the cantilever beam and the four-edge fixed plate with full coverage constraint damping. The optimisation results of the cantilever beam show that the damping treatment is distributed at the constraint end when the first-order modal loss factor is taken as the target. Also, it is distributed at the constrained end and both sides of the cantilever beam when the second-order modal loss factor is the optimisation target. When the material consumption is 50% of full coverage, after optimisation, the first- and second-order modal loss factors are reduced by 0.03% and 41.65%, respectively. The optimisation results of the four-edge fixed plate show that the damping treatment is mainly distributed in the middle of the plate when the first- and second-order modal loss factors are taken as the optimisation target. After optimisation, the first-

and second-order modal loss factor is reduced by 30.07% and 26.15%, respectively. The optimisation results are verified by experiments. The results are in good agreement with the optimisation results. Through the layout optimisation of constrained damping, the additional mass and vibration response of the damping structure is reduced effectively.

(3) Applying the BESO method to constrained damping layout topology optimization can delete inefficient damping elements and restore those efficient but deleted elements to solid elements during the optimization process. Then, the optimization results are more reasonable. The proposed constrained damping topology optimisation program based on the BESO method is effective, practical and easy to co-simulate with the commercial finite element analysis software. It has good guiding significance in the constrained damping design of thin-walled structures in the engineering fields of automobile, aircraft cabin, submarine shell and the like.

REFERENCES

- [1] D. Marco, V. Davide, and N. Guido, "Modal methodology for the simulation and optimization of the free-layer damping treatment of a car body," *Journal of Vibration and Acoustics*, vol. 132, no.2, pp. 1-8, 2010
- [2] L. Steinbach, and M. E. Altinsoy, "Prediction of annoyance evaluations of electric vehicle noise by using artificial neural networks," *Applied Acoustics*, vol. 145, pp. 149-158, 2019
- [3] H. B. Huang, X. R. Huang, M. L. Yang, T. C. Lim, and W. P. Ding, "Identification of vehicle interior noise sources based on wavelet transform and partial coherence analysis," *Mechanical Systems and Signal Processing*, vol. 109, pp. 247-267, 2018
- [4] Q. Feng, L. M. Fan, L. S. Huo, and G. B. Song, "Vibration reduction of an existing glass window through a viscoelastic material-based retrofit," *Applied Sciences*, vol. 8, no.7, pp. 1-13, 2018
- [5] R. M. Kanasogi, and M. C. Ray, "Active constrained layer damping of smart skew laminated composite plates using 1-3 piezoelectric composites," *Journal of Composites*, vol. 2013, pp. 1-17, 2013
- [6] Z. C. Huang, X. G. Wang, N. X. Wu, F. L. Chu, and J. Luo, "A finite element model for the vibration analysis of sandwich beam with frequency-dependent viscoelastic material core," *Materials*, vol. 12, no.20, pp. 1-16, 2019
- [7] L. Zheng, Q. Qiu, H. C. Wan, and D. D. Zhang, "Damping analysis of multilayer passive constrained layer damping on cylindrical shell using transfer function method," *Journal of Vibration and Acoustics*, vol. 136, no.3, pp. 1-9, 2014
- [8] N. Kumar, and S. P. Singh, "Experimental study on vibration and damping of curved panel treated with constrained viscoelastic layer," *Composite Structures*, vol. 92, no.2, pp. 233-243, 2010
- [9] G. Lepoittevin, and G. Kress, "Optimization of segmented constrained layer damping with mathematical programming using strain energy analysis and modal data," *Materials & Design*, vol. 31, no.1, pp. 14-24,

2010

- [10] A. Alaimo, C. Orlando, and S. Valvano, "Analytical frequency response solution for composite plates embedding viscoelastic layers," *Aerospace Science and Technology*, vol. 92, pp. 429-445, 2019
- [11] W. D. Yuan, Z. Gao, H. K. Liu, and G. F. Miu, "Topology optimization of composite shell damping structures based on improved optimal criteria method," *Acta Aeronautica et Astronautica Sinica*, vol. 41, no.1, pp. 191-202, 2020
- [12] T. Yamamoto, T. Yamada, K. Izui, and S. Nishiwaki, "Topology optimization of free-layer damping material on a thin panel for maximizing modal loss factors expressed by only real eigenvalues," *Journal of Sound and Vibration*, vol. 358, pp. 84-96, 2015
- [13] L. Zheng, R. L. Xie, Y. Wang, and E. Adel, "Topology optimization of constrained layer damping on plates using method of moving asymptote (MMA) approach," *Shock and Vibration*, vol. 18, no.1, 2, pp. 221-244, 2011
- [14] W. G. Zheng, Y. F. Lei, S. D. Li, and Q. B. Huang, "Topology optimization of passive constrained layer damping with partial coverage on plate," *Shock and Vibration*, vol. 20, no.2, pp. 199-211, 2013
- [15] M. Ansari, A. Khajepour, and E. Esmailzadeh, "Application of level set method to optimal vibration control of plate structures," *Journal of Sound and Vibration*, vol. 332, no.4, pp. 687-700, 2013
- [16] H. L. Simonetti, V. S. Almeida, and L. D. O. Neto, "A smooth evolutionary structural optimization procedure applied to plane stress problem," *Engineering structures*, vol. 75, pp. 248-258, 2014
- [17] L. Y. Chen, and Y. F. Zhang, "The study of structural dynamical optimization based on modified evolutionary structural optimization approach," *Journal of Vibration Engineering*, vol. 27, no.1, pp. 46-50, 2014
- [18] Y. N. Li, R. L. Xie, Y. Wang, and L. Zheng, "Topology optimization for constrained layer damping material in structures using ESO method," *Journal of Chongqing University*, vol. 33, no.8, pp. 1-6, 2010
- [19] D. J. Munk, G. A. Vio, and G. P. Steven, "A bi-directional evolutionary structural optimisation algorithm with an added connectivity constraint," *Finite Elements in Analysis and Design*, vol. 131, pp. 25-42, 2017
- [20] X. Wang, H. L. Liu, K. Long, D. Yang, and P. Hu, "Stress-constrained topology optimization based on improved bi-directional evolutionary optimization method," *Chinese Journal of Theoretical and Applied Mechanics*, vol. 50, no.2, pp. 385-394, 2018
- [21] B. Xu, J. S. Jiang, and Y. M. Xie, "Concurrent design of composite macrostructure and multi-phase material microstructure for minimum dynamic compliance," *Composite Structures*, vol. 128, pp. 221-233, 2015
- [22] J. S. Moita, A. L. Araújo, C. M. M. Soares, and C. a. M. Soares, "Finite element model for damping optimization of viscoelastic sandwich structures," *Advances in Engineering Software*, vol. 66, pp. 34-39, 2013
- [23] A. El-Sabbagh, and A. Baz, "Topology optimization of unconstrained damping treatments for plates," *Engineering optimization*, vol. 46, no.9, pp. 1153-1168, 2014
- [24] A. E. Alshorbagy, M. A. Eltahir, and F. F. Mahmoud, "Free vibration characteristics of a functionally graded beam by finite element method," *Applied Mathematical Modelling*, vol. 35, no.1, pp. 412-425, 2011
- [25] V. Shobeiri, "Topology optimization using bi-directional evolutionary structural optimization based on the element-free Galerkin method," *Engineering optimization*, vol. 48, no.3, pp. 380-396, 2016
- [26] Z. F. Zhang, X. S. Ni, Z. M. Xu, Y. S. He, Q. Yuan, and et al, "Topologic optimization of a free damping material based on optimal criteria method," *Journal of Vibration and Shock*, vol. 32, no.14, pp. 98-102, 2013
- [27] A. Aremu, I. Ashcroft, R. Wildman, R. Hague, C. Tuck, and et al, "The effects of bidirectional evolutionary structural optimization parameters on an industrial designed component for additive manufacture," *Proceedings of the Institution of Mechanical Engineers, Part B: Journal of Engineering Manufacture*, vol. 227, no.6, pp. 794-807, 2013
- [28] L. Xia, Q. Xia, X. D. Huang, and Y. M. Xie, "Bi-directional evolutionary structural optimization on advanced structures and materials: a comprehensive review," *Archives of Computational Methods in Engineering*, vol. 25, no.2, pp. 437-478, 2018